Behavioral/Systems/Cognitive

TASK Channels Contribute to the K^+-Dominated Leak Current Regulating Respiratory Rhythm Generation *In Vitro*

Hidehiko Koizumi,[1,2]* Stanley E. Smerin,[1]* Tadashi Yamanishi,[1]* Bindiya R. Moorjani,[1] Ruli Zhang,[1] and Jeffrey C. Smith[1]

[1]Cellular and Systems Neurobiology Section, National Institute of Neurological Disorders and Stroke, National Institutes of Health, Bethesda, Maryland 20892, and [2]Osaka University Graduate School of Dentistry, Osaka 565-0871, Japan

Leak channels regulate neuronal activity and excitability. Determining which leak channels exist in neurons and how they control electrophysiological behavior is fundamental. Here we investigated TASK channels, members of the two-pore domain K^+ channel family, as a component of the K^+-dominated leak conductance that controls and modulates rhythm generation at cellular and network levels in the mammalian pre-Bötzinger complex (pre-BötC), an excitatory network of neurons in the medulla critically involved in respiratory rhythmogenesis. By voltage-clamp analyses of pre-BötC neuronal current–voltage (I-V) relations in neonatal rat medullary slices *in vitro*, we demonstrated that pre-BötC inspiratory neurons have a weakly outward-rectifying total leak conductance with reversal potential that was depolarized by ~4 mV from the K^+ equilibrium potential, indicating that background K^+ channels are dominant contributors to leak. This K^+ channel component had I-V relations described by constant field theory, and the conductance was reduced by acid and was augmented by the volatile anesthetic halothane, which are all hallmarks of TASK. We established by single-cell RT-PCR that pre-BötC inspiratory neurons express TASK-1 and in some cases also TASK-3 mRNA. Furthermore, acid depolarized and augmented bursting frequency of pre-BötC inspiratory neurons with intrinsic bursting properties. Microinfusion of acidified solutions into the rhythmically active pre-BötC network increased network bursting frequency, halothane decreased bursting frequency, and acid reversed the depressant effects of halothane, consistent with modulation of network activity by TASK channels. We conclude that TASK-like channels play a major functional role in chemosensory modulation of respiratory rhythm generation in the pre-Bötzinger complex *in vitro*.

Introduction

Leak or background channels determine neuronal resting membrane potentials, regulate excitability, and control electrophysiological behavior. Multiple channels mediate leak currents, including channels with mixed cationic permeabilities (Lu et al., 2007) and specific types of K^+ channels such as TASK channels, members of the family of two-pore domain K^+ (K_{2P}) channels (Lesage and Lazdunski, 2000). TASK-1 and TASK-3, two forms of TASK present in mammalian brain (Medhurst et al., 2001; Mulkey et al., 2007), like other background channels, are targets for neuromodulation (Talley et al., 2000; Mathie, 2007). Identifying which leak channels exist in different neurons and how they regulate electrophysiological behavior including via neuromodulation is fundamental.

Here we identified TASK-like channels and examined their role in regulation of rhythm generation within the brainstem respiratory pre-Bötzinger complex (pre-BötC) (Smith et al., 1991; Gray et al., 2001), a region of the mammalian medulla containing a heterogeneous excitatory network that is the substrate for inspiratory rhythm generation (Smith et al., 2000; Feldman and Del Negro, 2006). This network has autorhythmic properties (Johnson et al., 2001) and remains active in neonatal rodent medullary slice preparations, allowing analyses of cellular and network mechanisms of rhythmogenesis *in vitro* (Smith et al., 1991; Koshiya and Smith, 1999; Del Negro et al., 2001). We have proposed (Butera et al., 1999a,b), and found experimentally (Koizumi and Smith, 2008), that a K^+-dominated leak conductance plays a fundamental role in generation and control of pre-BötC rhythmic activity *in vitro*.

Channels mediating this conductance, however, have not been identified. We hypothesized that TASK channels contribute based on known biophysical and chemosensitive properties. TASK channels have neuronal current–voltage (I-V) relations that fit constant field theory for simple electrodiffusion through an open K^+-selective pore (Leonoudakis et al., 1998), consistent with our observations of pre-BötC neuronal leak I-V properties (Koizumi and Smith, 2008). Furthermore, the pre-BötC network is hypothesized to have chemosensitive properties (Solomon et al., 2000; Nattie, 2001). TASK channels close in response to extracellular acidification (Duprat et al., 1997; Rajan et al., 2000). A further chemosensitivity is that TASK channels open in response to halothane (Talley and Bayliss, 2002) and other volatile anesthetics (Bayliss et al., 2003). Thus TASK may contribute to pre-BötC neuronal pH-related chemosensory properties and suppression of rhythmic breathing by volatile anesthetics. Mod-

Received Aug. 14, 2009; revised Jan. 14, 2010; accepted Feb. 1, 2010.

This research was supported by the Intramural Research Program of the National Institute of Neurological Disorders and Stroke, National Institutes of Health. We thank Murtaza Mogri for scripting modeling simulations.

*H.K., S.E.S., and T.Y. contributed equally to this work.

Correspondence should be addressed to Dr. Jeffrey C. Smith, Senior Investigator and Chief, Cellular and Systems Neurobiology Section, Building 49, Room 2A10, NINDS, NIH, Bethesda, MD 20892-3700. E-mail: jsmith@ helix.nih.gov.

DOI:10.1523/JNEUROSCI.4017-09.2010

 0270-6474/10/304273-12$15.00/0

ulation of pre-BötC leak currents by serotonin and substance P, two important neuromodulators of rhythmogenesis, is mediated in part by TASK-like and by nonselective cationic NALCN-like conductance components (Lu et al., 2007, 2009; Hayes and Del Negro, 2007; Ptak et al., 2009), suggesting a critical neuromodulatory role of TASK.

The four properties of TASK channels, selectivity for K^+, I-V relations described by constant field theory, closure to extracellular acid, and opening to halothane, differentiate TASK from all other known channels. We used these properties to probe for TASK channels in pre-BötC inspiratory neurons in rhythmically active neonatal rat brainstem slices *in vitro*. Augmentation of TASK-like conductance by halothane downregulated, and reductions in conductance by extracellular acid augmented, rhythm generation at cellular and network levels, implying a functional role of TASK channels in pre-BötC chemoreception and respiratory rhythm generation *in vitro*.

Materials and Methods

Thin slice preparations

Transverse slices (250 to 350 μm thick) of medulla oblongata were cut from Sprague Dawley neonatal (P0 to P4) rats to contain the pre-BötC and rostral end of the hypoglossal (XII) motor nucleus including XII nerve rootlets as previously described (Koshiya and Smith, 1999; Koizumi and Smith, 2008). All animal use procedures were approved by the institutional Animal Care and Use Committee of the National Institute of Neurological Disorders and Stroke (NINDS), National Institutes of Health (NIH; approved ASP #1154-06). The caudal surface of the slice was cut through the caudal pre-BötC for imaging and recording neuronal activity. The slice was oriented caudal end up in a recording chamber (0.2 ml) mounted on the stage of an upright microscope, anchored in the chamber by nylon fibers attached to an overlying platinum ring, and superfused (4 ml/min) with artificial cerebrospinal fluid (aCSF) containing (in mM) 124 NaCl, 25 $NaHCO_3$, 3 KCl, 1.5 $CaCl_2$, 1.0 $MgSO_4$, 0.5 NaH_2PO_4, 30 D-glucose and antibiotics (500 units/l penicillin, 0.5 mg/l streptomycin and 1 mg/l neomycin), equilibrated with 95% O_2 and 5% CO_2 (pH = 7.35 to 7.40 at 27°C). Rhythmic respiratory network activity recorded from XII nerves was maintained by elevating the superfusate K^+ concentration (8 mM).

Pharmacologic procedures

Pharmacological agents [tetrodotoxin (TTX, Sigma-RBI), ZD7288 (Tocris Bioscience), 6-cyano-7-nitroquinoxaline-2,3-dione disodium (CNQX, Sigma), barium chloride (Ba^{2+}, Sigma), tetraethyl ammonium chloride (TEA, Sigma), and/or cadmium chloride (Cd^{2+}, Sigma)], were dissolved in the standard perfusion solution with elevated K^+ concentration. Acidified aCSF (pH 7.2, 7.0, 6.8, 6.5, 6.0) was prepared by decreasing the concentration of $NaHCO_3$ in the aCSF; osmolarity was maintained by increasing the concentration of NaCl. The aCSF was equilibrated by continuous bubbling with halothane delivered by a calibrated vaporizer (Fluotec, Surgivet), with vaporizer settings of 0.25% to 2.0%. From our functional assays this produced effective concentrations in the slice bathing solution that progressively and reversibly depressed pre-BötC neuronal or network rhythmic activity in a concentration-dependent manner, and also reversibly augmented leak conductance as found for other CNS neurons where the same percentage gas compositions were used and gas chromatographic analysis demonstrated aqueous anesthetic concentrations within expected ranges for anesthetic efficacy (Sirois et al., 2000). In some experiments the aCSF was equilibrated with isoflurane delivered by a separate calibrated vaporizer (Isotec, Surgivet) with vaporizer settings of 0.5% to 2.0%. In all cases the perfusion solutions were delivered to the bath (4 ml/min) through a short segment of gas-impermeable tubing to minimize loss of the anesthetic. We therefore denote the anesthetic compositions of our slice bathing solution by the percentage of vaporized anesthetic equilibrated with the perfusate.

Microinfusion in the pre-BötC

Acidified aCSF or halothane equilibrated aCSF, prepared as above, was loaded into a polished glass pipette (~10 μm tip diameter), positioned 100 to 200 μm deep into the core of the pre-BötC (depending on slice thickness) (see Fig. 1), and continuously infused convectively, to minimize local concentration gradients, by applying low pressure (~10 to 20 mmHg) to the pipette with a precision pressure control and valve system (Picospritzer-IID, General Valve Corp, and 2PK+ Pressure Controller, ALA Scientific Instruments). This system allowed us to precisely control convective microdelivery of anesthetic-containing or acidic aCSF locally within the imaged locus of pre-BötC network activity (Koizumi and Smith, 2008). For the typical microinfusion rate (10 nl-min^{-1}) used, we estimate that the infusate would spread by convection and have effective concentrations over a region of ~200 to 300 μm in diameter, which would encompass the pre-BötC region on each side (see Fig. 1). This was tested in some experiments by microinfusing the halothane- or acid-containing solution at the same rate adjacent to the pre-BötC by positioning the infusion pipette tip at the same depth in the tissue but 200 μm from the boundary of the imaged pre-BötC region. These infusions did not cause any perturbations of network activity, indicating that we could achieve site-specificity with our microinfusion procedures when applied to the pre-BötC.

Imaging pre-BötC rhythmic neuronal activity

We imaged rhythmic Ca^{2+} fluorescence transients of inspiratory neurons to map the location of the pre-BötC at the level of population activity for microinfusion experiments (Koizumi and Smith, 2008) and individual neurons for whole-cell patch-clamp recording. Methods for retrograde labeling of pre-BötC neurons with Ca^{2+}-sensitive dye and imaging were as previously described (Koshiya and Smith, 1999; Koizumi et al., 2008). Briefly, membrane-permeant Ca^{2+}-sensitive dye, Calcium Green-1 AM (CaG; Invitrogen, 50 μg), dissolved in 5 μl of DMSO containing 25 μg of pluronic F-127 (BASF) and dispersed in 10 μl of aCSF, was microinjected with a glass pipette (~10 μm tip diameter) into the slice near the midline to retrogradely label bilaterally pre-BötC neurons overnight (8 to 12 h). CaG-labeled inspiratory neurons were visualized with a fixed-stage upright microscope (Axioskop-FS1or FS2, Zeiss) with a 75 W xenon epi-illuminator, optical filters (excitation 485 nm, emission 530 nm, and beam splitter 505 nm, Omega Optical), and a 63× water-immersion objective (Zeiss Achroplan, N.A. 0.95). Fluorescence images were captured with a CCD camera fiber-optically coupled to a fluorescence image-intensifying camera (ICCD-1000F, VideoScope International) and recorded on videotape and digitized together with electrophysiological signals. Changes in fluorescence intensity ($\Delta F/F$) were detected in real time with an image processor (ARGUS 20, Hamamatsu Photonics) and quantified off-line after digitizing images using an audio-video board (SONY Media Converter). Inspiratory population and single neuron "flash" images were obtained by subtracting baseline CaG fluorescent images from images acquired during peak inspiratory activity with an image processor in real time and displayed in pseudocolor. Simultaneous videomicroscopic infrared differential interference contrast (IR-DIC) imaging was done using 900 nm infrared illumination, a wide spectrum polarizer (Melles Griot), and an 850 to 950 nm analyzer (Polarcor, Corning). The IR-DIC image was captured with an extended IR Newvicon camera (Hamamatsu Photonics), and enhanced with the ARGUS 20 in real time. For dual imaging, the Newvicon and ICCD cameras were mounted on a dual-port imaging head incorporating a dichroic beam splitter (700 nm, Zeiss), and images were aligned by reverse scanning and scan range shifting of the Newvicon camera.

Electrophysiological recording and data acquisition

Neuron population activity. XII motoneuron population activity, used to monitor inspiratory network activity in the slices (see Fig. 1), was recorded with fire-polished glass suction electrodes (60 to 90 μm inner diameter), amplified (5000 to 10,000X, CyberAmp 380, Molecular Devices), bandpass filtered (0.3 to 2 kHz), digitized (10 kHz) with an AD converter (Power Lab, AD Instruments), and then rectified and integrated ($\int$XII) by either an analog integrator or digitally via software (Chart software, ADInstruments). Measurements of parameters of net-

work population activity (inspiratory population burst frequency) were made offline with custom automated algorithms in Chart software (AD Instruments) and Igor Pro (Wavemetrics) for XII inspiratory burst detection and hand-checked for accuracy. All data presented as burst frequency were first analyzed by computing burst period, defined as the interval from onset to onset of consecutive inspiratory bursts.

Whole-cell current and voltage-clamp recordings. Voltage- and current-clamp data obtained from whole-cell patch-clamp pipette electrodes were recorded with a HEKA EPC-9 amplifier controlled by Pulse or PatchMaster software (HEKA; 2.8 kHz low-pass filter). Borosilicate recording electrodes (4 to 6 MΩ), positioned with microdrives (Sutter Instrument or SDInstruments), contained (in mM): 130.0 K-gluconate, 10.0 Na-gluconate, 4.0 NaCl, 10.0 HEPES, 4.0 Mg-ATP, 0.3 Na-GTP, and 4.0 sodium phosphocreatine, adjusted with NaOH to match the intracellular pH (7.3, Filosa et al., 2002; Putnam et al., 2004). Rhythmically active neurons were identified by CaG fluorescence transients as described above. In some experiments where indicated, we alternatively used blind whole-cell patch-clamp recording to include in the sample neurons deeper in the slice (>90 μm below the slice surface) beyond the limits of optical resolution. In all cases measured potentials were corrected for the liquid junction potential (−10 mV). To identify intrinsic oscillatory bursting neurons, excitatory synaptic transmission was blocked with 20 μM CNQX or by the calcium channel blocker Cd^{2+} (200 μM). To control for non-K_{2P} currents during measurement of cellular leak conductance, in some experiments sodium channels as well as synaptic currents were blocked with TTX (1 μM), inwardly rectifying K^+ conductance (Kir) was blocked with barium (200 μM), K_v^+ channels with TEA (10 mM), voltage-gated Ca^{2+} channels with cadmium (200 μM), and h-current (I_h) with ZD7288 (100 μM) (Shin et al., 2001), all dissolved in the slice perfusate solution.

Measurements of neuronal burst frequency in current clamp were made offline with Chart software and Igor Pro. All data presented as neuronal burst frequency were analyzed by computing burst period with spike detection algorithms, and subsequent computation of burst frequency was done similar to that for population activity as described above.

Voltage-dependence of whole-cell currents was analyzed from voltage-clamp data using Pulsefit, Chart, and Igor Pro software. Neuronal membrane leak conductance (gLeak) was determined from measurements of leak currents using slow voltage ramps (30 mV/s, −110 mV to +10 mV) applied in voltage clamp. Leak conductances were calculated in a data analysis program (Igor Pro) by linear regression to the slope of the essentially linear region of the membrane I-V curve (−100 mV to −65 mV). Cell capacitance (Cm) was determined from the integral of the transient capacitance current (I_C, leak subtracted) evoked by a 15 ms hyperpolarizing voltage-step command applied within −10 mV of resting potential, using $\int I_C dt = -Qm$ at each command potential (Vm). Cm was determined from the slope of the plot of Qm versus ΔVm for the series of step commands. Series resistance (R_S) was calculated from the decay-time constant of I_C, and compensated online by ≥80%. Neurons failing to meet the criterion Rm >10 R_S necessary to achieve space clamp were excluded from voltage-clamp analysis. Furthermore, neurons with clear evidence of poor space clamp such as unclamped action potential currents during the slow voltage-clamp ramps were excluded from the analysis. Statistical significance was determined by a Student paired *t* test on mean data. Data are presented as means ± SE unless otherwise indicated.

K^+ equilibrium potential and fit of the Goldman-Hodgkin-Katz equation to the K^+ leak I-V relation

K^+ equilibrium potential (E_K) was calculated from the Nernst equation, $E_K = -RT/F \ln[K]_O/[K]_I$, which yielded values of $E_K = -72$ mV, for the intracellular recording and extracellular solution K^+ concentrations ($[K]_O = 8$ mM, $[K]_I = 125$ mM), and $RT/F = 25.86$ at 27°C (Hille, 2001). This value was compared to the membrane voltages at the intersection of the whole-cell I-V ramps for control and experimental (acid or halothane) conditions to assess whether the equilibrium potential for the channel affected was consistent with E_K.

The Goldman-Hodgkin-Katz (GHK) equation for simple electrodiffusion of K^+ may be written as: $I_K = P_K (F^2 V_m/RT)(([K_I] - [K_O] \exp(-FV/RT))/(1 - \exp(-FV/RT))$ (Hille, 2001), where P_K is the membrane permeability to K^+. Because the constant that relates P_K to K^+ channel conductance is not known, P_K was treated as a constant of proportionality. Substituting terms $V_m = -110$ mV to 10 mV, $[K]_I = 125$ mM, $[K]_O = 8$ mM, F/RT @ 27°C = 0.0385 mV^{-1} (Hille, 2001), yields the GHK equation as a proportionality between I_K and V_m: $I_K \propto V_m(17\exp(-0.0385V_m))/(1 - \exp(-0.0385V_m))$; this proportionality was then graphed over the voltage range −110 to 10 mV and fit to the I-V curve for leak current by scaling I_K.

Single-cell multiplex RT-PCR

For single-cell (sc) RT-PCR experiments, at the end of the whole-cell recording session, the cytoplasm was aspirated as completely as possible into the patch pipette under visual control and then immediately expelled into a thin-walled PCR tube containing reverse transcription reagents (Invitrogen Life Technologies). First strand cDNA was synthesized for 1.5 h at 50°C in a mixture of MgCl (2 μl, 25 mM), dNTPs (1 μl, 10 mM), BSA (0.7 μl, 143 ng/μl), random hexamers (1 μl, 50 ng/μl), oligodT (0.7 μl, 0.5 μg/μl), RNasin (1.2 μl, 40 u/μl), DTT (1 μl, 0.1 M), and SuperScriptIII RT (1 μl, 200 u/μl). The entire reaction was either immediately used as template for multiplex PCR or frozen at −80°C until assayed.

After reverse transcription, the cDNAs for TASK-1 and/or TASK-3 were amplified simultaneously with a multiplex PCR procedure using the following set of primers (from 5′ to 3′): TASK-1 (GenBank accession # AFO31384) sense, CAC CGT CAT CAC CAC AAT CG (position 367 to 386), antisense, TGC TCT GCA TCA CGC TTC TC (position 882-863); TASK 3 (GenBank accession # NM053405) sense, ATG AAG CGG CAG AAT GTG CG (position 91 to 110), antisense, AGA AGA TCT TCA TCG GTA TT (position 854 to 835). The first multiplex PCR was performed as hot start in a final volume of 50 μl containing 12 μl reverse transcription reaction, 20 to 50 pmol of each primer, 0.2 mM dNTPs, 10× High Fidelity PCR buffer with 2 mM $MgCl_2$, and 5 U of Platinum Taq High Fidelity DNA polymerase (Invitrogen Life Technologies). The reaction mixtures were heated to 94°C for 2 min, 30 cycles (94°C, 30 s; 55°C, 30 s; 68°C, 1 min) of PCR followed by a final elongation period of 10 min at 68°C. The second round of PCR amplification was performed as individual reactions with individual primers, using 1 μl of the first PCR reaction product under similar conditions with the following modifications: 50 pmole of each primer pair and 25 thermal cycles. Ten microliter aliquots of PCR products were separated and visualized in an ethidium bromide-stained agarose gel (2%) by electrophoresis. The expected sizes of PCR-generated fragments were: TASK-1 (515 bp) and TASK-3 (763 bp).

To ensure that the PCR signal arose from the cytoplasm of the recorded cell, in each experiment we performed 'mock harvests' whereby a pipette was introduced into the slice but no cell contents extracted, and RT-PCR assays were run on harvested pipette solution as described above as negative controls from each brain slice. In all scRT-PCR assays 100 pg total rat brain RNA (Ambion) was also run as RT template to serve as a positive control.

Cellular and network modeling methods

To theoretically examine and gain insight into regulation of intrinsic bursting and network oscillations of pre-BötC neurons by modulation of TASK-like leak conductances, we used our previous neuron models consisting of a single somal compartment incorporating a fast-activating slowly inactivating persistent Na^+ conductance (gNaP) and a K^+-dominated ohmic leak conductance (gLeak) for the two major neuronal subthreshold currents as measured here and elsewhere (Koizumi and Smith, 2008), as well as Hodgkin-Huxley-like transient Na^+ current and delayed-rectifier-like K^+ current for action potential generation, as previously described in detail (Model 1) (Butera et al., 1999a; Del Negro et al., 2001). The pre-BötC excitatory network was modeled by 50 synaptically-coupled (Butera et al., 1999b) neurons with fast glutamatergic (AMPA)-like synaptic currents, and heterogeneous parameter values (below) that produced a mixture of cells with intrinsic and nonintrinsic bursting properties when synaptic conductance was set to zero (synaptically uncoupled), which is consistent with experimental observations that only a fraction of pre-BötC neurons exhibit intrinsic bursting prop-

erties when synaptic transmission is blocked (Koshiya and Smith, 1999; Purvis et al., 2007; Koizumi and Smith, 2008). Except for NaP steady-state activation properties, neuron capacitance values, and E_K, all other Model 1 current parameters as well as parameters for phasic excitatory synaptic currents were identical to those specified previously (Butera et al., 1999a, 1999b). Steady-state activation properties for NaP used were based on Boltzmann function data obtained in our previous study (Koizumi et al., 2008) ($V_{1/2max} = -47$ mV, k = 5.0); similarly data-based Cm (28 nS), and E_K (−72 mV) values as calculated from the intra- and extracellular K^+ concentrations under the present recording conditions, were used. The networks also incorporated a small constant background tonic postsynaptic excitatory conductance as previously described (Butera et al., 1999b), which was set at 0.1 nS. All simulations used all-to-all synaptic coupling for the 50 cells, the smallest population that preserves the dynamics observed for populations an order of magnitude larger (Butera et al., 1999b; Purvis et al., 2007). To incorporate parameter heterogeneity, neuronal gNaP, gLeak, and excitatory post-synaptic conductance values were randomly assigned within the network population from normal distributions with ±30% SD for each parameter to mimic our experimental data (Purvis et al., 2007). Total neuronal leak conductance (gLeak) was partitioned into a dominant K^+ component ($gLeak_K$) and a small fixed cationic leak component as previously described (Del Negro et al., 2001; Koizumi and Smith, 2008). Numerical methods were identical to those described previously (Butera et al., 1999b), and simulations were run with Berkeley Madonna software. The initial 20 s of simulated time (typically 90 s total) was discarded. Network activity was displayed and analyzed from running histograms (adjustable bin size: 10 to 100 ms) of spike times computed and averaged across the population. Raster plots of neuron spiking (Butera et al., 1999b; Purvis et al., 2007) were used to assess neuronal burst synchronization within the network and stability of the network rhythm.

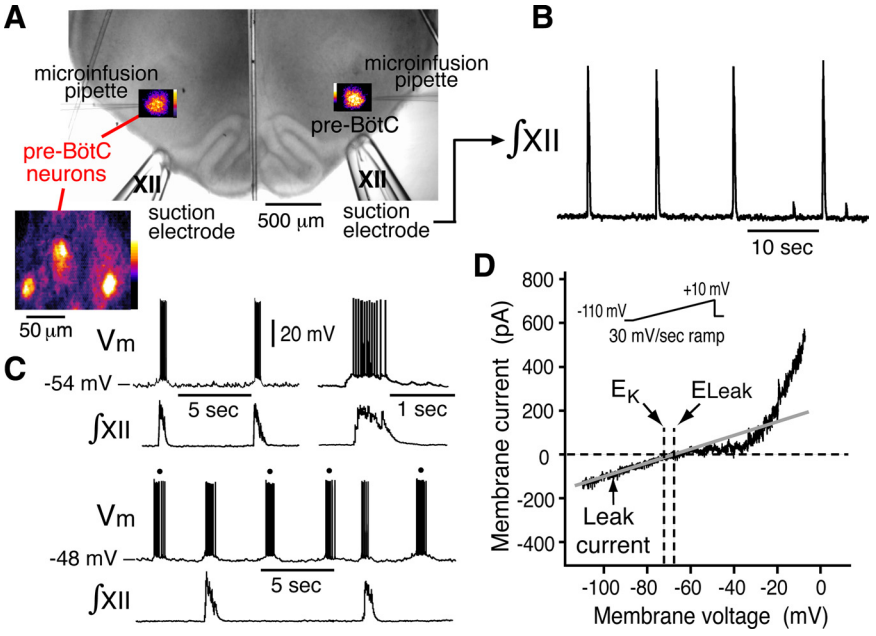

Figure 1. Overview of experimental *in vitro* neonatal rat rhythmic slice preparation with inspiratory neuronal imaging, set-up for local microinfusion in the pre-BötC, and representative current- and voltage-clamp recordings of functionally identified inspiratory neurons *in vitro*. ***A***, ***B***, Glass pipette suction electrodes on hypoglossal (XII) nerves (***A***) were used to bilaterally record inspiratory motoneuronal population discharge (***B***, integrated population activity ∫XII) as a monitor respiratory network rhythmic activity. Inspiratory neurons were localized for whole-cell recording in the pre-BötC by imaging single-neuron (box at lower left, ×63 magnification) and population fluorescence transients (pseudo-colored fluorescence flash images shown in ***A***), produced by inspiratory activity of neurons retrogradely labeled with the Ca^{2+}-sensitive dye Calcium Green-1 AM (see Materials and Methods for detailed explanation). Imaged population activity (×20 fluorescence population flash images shown superimposed bilaterally on IR-DIC image of ventral half of slice in ***A***) was also used to locate the core of active pre-BötC inspiratory neurons to guide insertion of micropipettes into the center of the inspiratory population for local microinfusion of aCSF containing acid or halothane. ***C***, Imaged pre-BötC inspiratory neurons were recorded in current-clamp and further identified functionally by rhythmic bursting in synchrony with XII motor discharge. Neurons with intrinsic voltage-dependent bursting properties (bottom traces in ***C***) were initially identified and distinguished from nonintrinsic bursters by rhythmic ectopic bursting (marked by dots above bursts) unsynchronized with XII discharge when the neuronal membrane potential (Vm) was depolarized by steady current injection. ***D***, I-V relations of identified inspiratory neurons were measured by a voltage-clamp ramp protocol (30 mV/s ramp) with synaptic transmission blocked under control conditions and after bath-application of acidified aCSF and/or aCSF containing halothane. I-V relation for a nonintrinsic burster neuron is shown. Leak I-V relations, used to calculate leak conductances, were determined from linear regression (solid gray line shown) to the passive regions (below −65 mV) of I-V curves. The reversal potential, ELeak, of the total leak current (0 current intercept of regression line), is indicated by the vertical dashed line and was typically depolarized from the calculated K^+ equilibrium potential (E_K indicated) for the recording conditions.

Results

Pre-Bötzinger complex inspiratory neurons have a TASK-like component of leak current

To determine whether pre-BötC inspiratory neurons have TASK, we first tested functionally identified pre-BötC inspiratory neurons in isolated rhythmically-active *in vitro* neonatal rat slice preparations for the four electrophysiological properties of TASK channels: selectivity for K^+, whole-cell I-V relations described by constant field theory, channel closure to extracellular acid, and channel opening to halothane.

We labeled and imaged rhythmically active pre-BötC inspiratory neurons in the slices with Ca^{2+}-sensitive dye (CaG) (Fig. 1*A*), allowing functional identification of cells for targeted whole-cell patch-clamp recording. All neurons analyzed ($n = 78$) exhibited spike discharge synchronized with the rhythmic motoneuronal population activity recorded from hypoglossal (XII) nerve roots (Fig. 1*B*), which was used to monitor inspiratory network activity in the slices (Koshiya and Smith, 1999; Koizumi and Smith, 2008). To functionally isolate the cells for voltage-clamp analysis of membrane currents, we blocked synaptic transmission by either bath-applied Cd^{2+} (200 μM) or the non-NMDA glutamate receptor antagonist CNQX (20 μM), which eliminated rhythmic excitatory synaptic drive currents (Koshiya and Smith, 1999). These inspiratory neurons had two distinct electrophysiological profiles: neurons exhibited either intrinsic voltage-dependent oscillatory bursting ($n = 47$), or only tonic spiking ($n = 31$ nonintrinsic bursters), when the baseline potential was depolarized after blocking excitatory synaptic transmission, as we have previously described (Koshiya and Smith, 1999; Del Negro et al., 2002). The intrinsic bursters were also revealed by ectopic bursting under current clamp before blocking synaptic transmission (Fig. 1*C*). For both types of cells, slow voltage-clamp ramps (30 mV/s, range: −110 to +10 mV) revealed that all neurons exhibited N-shaped I-V relations that could be decomposed into two primary subthreshold conductances: an ohmic-like conductance, evident by the essentially linear region of the I-V curve below −65 mV (with little if any rectification at hyperpolarized voltages), and a voltage-activated, TTX-sensitive, inward persistent Na^+ current (Del Negro et al., 2002; Koizumi and Smith, 2008) generating the negative slope region in the ~−60 mV to −40 mV

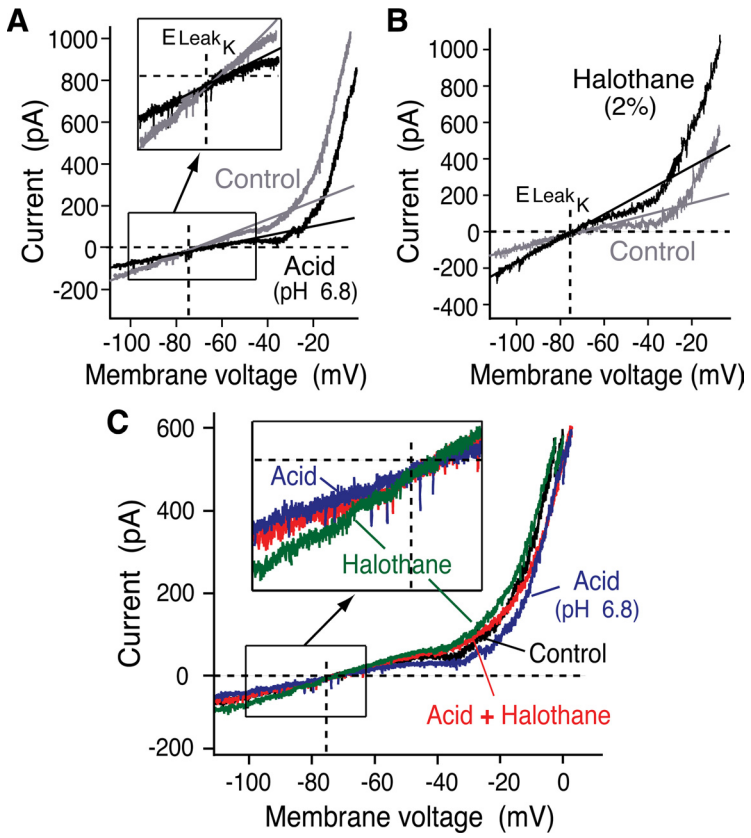

Figure 2. Acid decreases and halothane increases leak conductance of pre-BötC inspiratory neurons. ***A***, ***B***, Representative examples of whole-cell voltage-clamp ramp (30 mV/s) recordings of I-V relations of pre-BötC inspiratory neurons (data from nonintrinsic bursters in both panels) before (gray curves) and after (black) bath-application of acidic (pH = 6.8) aCSF (***A***) or halothane-containing aCSF (2%, ***B***), showing rotations of I-V relations about intersection at a membrane potential ($ELeak_K$) corresponding closely to E_K, which defines the K^+ component of the total leak current. Inset (box) in ***A*** shows expanded view of I-V rotation about $ELeak_K$ (indicated by vertical dashed lines in all panels). Leak conductance (gLeak) is indicated by slope of linear regression fits to the passive segment (−100 to −70 mV) of each I-V ramp (solid lines). In the examples shown, gLeak decreased by 1.0 nS or by 20% from control value with acid and increased by 3.5 nS (67% above control conductance) with halothane. ***C***, Acid (pH 6.8) reverses the increase of gLeak by halothane (green I-V relation) in a representative intrinsically bursting inspiratory neuron. Coapplication of acid (pH 6.8) + halothane (2%) (red curve) restores gLeak to that of control I-V relation (black); red I-V relation is superimposed on black curve in the inset showing expanded view of I-V relations at voltages below and above $ELeak_K$ over which gLeak was measured. Blue curve shows I-V relation during exposure to acid alone.

membrane voltage range. Leak conductance (gLeak) was determined by linear regression to the slope of the passive region (−110 to −65 mV) of the I-V relation (Fig. 1*D*). Under control conditions, the total leak current in all neurons examined had a reversal potential ELeak (0 current intercept of regression line) between −70 and −60 mV (mean ELeak = −68 ± 3.4 mV), similar to the potential previously determined for ELeak (Koizumi and Smith, 2008), which was at a slightly more depolarized membrane voltage that the calculated K^+ equilibrium potential (E_K), indicating as we found previously that gLeak was K^+-dominated, with a small non-K^+ cationic conductance component. We have suggested that the latter arises from a relatively small, open, nonselective cationic conductance (NALCN-like, Lu et al., 2007) with reversal potential between −10 and 0 mV (Koizumi and Smith, 2008; Ptak et al., 2009) and accounting for ~10% to 15% of gLeak under basal conditions.

We measured changes in gLeak in response to acid and/or halothane in functionally identified pre-BötC inspiratory neurons to test for contributions of a TASK-like K^+ conductance component of gLeak. Acidification of the slice bathing solution (pH = 6.8) decreased the slope of the I-V relation in the linear region dominated by gLeak (Fig. 2*A*) (n = 6 nonintrinsically bursting inspiratory neurons in this series). The mean gLeak decreased by 1.0 ± 0.4 nS or 24% from the control average conductance value of 3.9 ± 0.8 nS ($p < 0.0001$) as computed by linear regression (average 95% confidence interval of 1.6% for the linear fit). The I-V relation of the leak conductance and change in gLeak by acid was obtained by subtracting the I-V curves and slopes before and after acid. The current had an equilibrium potential ($ELeak_K$ in Fig. 2*A*) close to the calculated E_K for the intracellular-extracellular solution K^+ concentrations used (−73.9 ± 3.2 mV vs. −72 mV calculated, see Materials and Methods). The small (~2 mV) deviation of the experimentally determined equilibrium potential may be attributable to K^+ buffering in slices (Chen and Nicholson, 2000), with the $[K^+]_O$ surrounding the neurons recorded reduced from 8 mM (bath solution) to ~7 mM by buffering.

Halothane (1.0% to 2.0% in solution) (Fig. 2*B*) increased gLeak (n = 8 inspiratory neurons, with 2 intrinsic bursters) by 3.1 ± 1.5 nS or 66% above control values of 4.68 ± 2.7 nS ($p < 0.0003$) for this group of neurons (average increase of gLeak of 84.0% and 56.2% for nonintrinsic and intrinsic bursters, respectively). This halothane-sensitive leak current also had an equilibrium potential (−73.1 ± 2.8 mV) close to the calculated E_K, and the equilibrium potential was not significantly different ($p > 0.05$) from that found for the current affected by acid.

We also tested for interactions between acid and halothane (n = 6 inspiratory neurons, with 2 intrinsic bursters and 4 nonintrinsic bursters in this group). In all cases bath-applied acidic aCSF (pH 6.8) after halothane reversed the increase of gLeak by halothane (Fig. 2*C*, data from a representative intrinsic burster shown), which is characteristic of TASK channels (Bayliss et al., 2003). There were no obvious differences in the responses of intrinsic bursters and nonintrinsic bursters to halothane and acid, so the data for these two cell types were pooled. The mean gLeak with halothane (2%) increased in this group of neurons by 54% (from 2.9 ± 0.9 nS control values to 4.45 ± 1.47 nS, $p < 0.001$), and gLeak returned to 3.03 ± 1.04 nS with halothane + acid (pH 6.8), which was close to the control values.

To further characterize the I-V relations of gLeak, we bath-applied solutions with blockers of voltage-activated Na_v^+ (with 1 μM TTX), Ca^{2+} (with 200 μM Cd^{2+}), and K_v^+ channels (with 10 mM extracellular TEA) as well as nonselective cationic current I_h (with ZD7288, 100 μM) and other potential K^+ channel contributors to Leak such as inwardly rectifying K^+ conductances (Kir, blocked with 200 μM Ba^{2+}). Sirois et al. (2002) found a small effect of halothane in neurons attributable to I_h when they applied the I_h channel blocker ZD7288, and some Kirs are acid-sensitive (Zhu et al., 1999; Xu et al., 2000). The I-V relations

obtained in the presence of these blockers was linear at hyperpolarized voltages and exhibited slight outward rectification at depolarized voltages (Fig. 3). Nonintrinsic bursters (Fig. 3*A*) and intrinsic bursters (Fig. 3*B*) had similar I-V relations under these conditions, and responses of these two cell types to acid or halothane were also similar so data were again pooled for the groups exposed to acid or halothane. The mean gLeak in these neurons again decreased in response to acid on average by 22.6% and 25.6% at pH = 7.0 ($n = 2$, with 1 intrinsic burster) and 6.8 ($n = 3$, with 1 intrinsic burster), respectively, from control values in the presence of blockers (Fig. 3*A*). The average gLeak increased by 59.8% from control ($n = 4$, with 2 intrinsic bursters) in response to halothane (2%) (Fig. 3*B*). I-V relations of the affected conductance obtained by I-V curve subtraction in all cases conformed to the shape of the I-V curve predicted from GHK constant field theory (examples shown in Fig. 3*A*,*B*) for K^+ electrodiffusion through an open K^+-selective channel, and the mean reversal potentials ($ELeak_K$) for the acid and halothane affected conductance were not different (pooled values of -74.2 ± 3.4 mV for $ELeak_K$, $n = 9$) and were close to the calculated E_K.

To further validate our approach, we also measured I-V relations and the change in gLeak of inspiratory XII motoneurons (Koizumi et al., 2008) in response to bath-applied halothane solution (2%) in the slice preparations. Consistent with previous results that have demonstrated TASK channels in XII motoneurons (Sirois et al., 2000, 2002), we found that halothane increased gLeak of inspiratory XII motoneurons by an average of 57% (from control gLeak values of 9.64 ± 1.75 nS to 15.05 ± 2.72 nS, $n = 11$ inspiratory motoneurons; I-V data not shown).

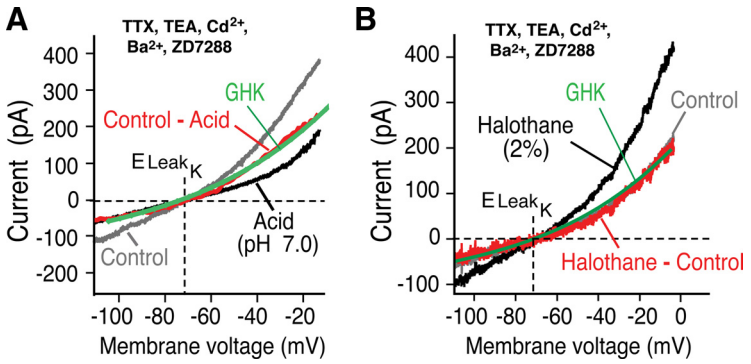

Figure 3. TASK-like leak I-V relations are fit by the curve predicted from constant field theory for electrodiffusion through an open K^+-selective pore. ***A***, ***B***, Representative ramp I-V relations of different inspiratory neurons (nonintrinsic burster in ***A***, intrinsic burster in ***B***) exposed to acidic aCSF (pH 7.0, ***A***) and aCSF containing halothane (2%, ***B***) when currents other than TASK are blocked. Na_v^+ channels were blocked with TTX (1 μM), Kir was blocked with Ba^{2+} (200 μM), K_v^+ with extracellular TEA (10 mM), Ca^{2+} channels with Cd^{2+} (200 μM), and I_h blocked with ZD7288 (100 μM). Difference I-V curves (red = control-acid in ***A***, red = halothane-control in ***B***) have a shape similar to the curve (green) calculated by the Goldman-Hodgkin-Katz (GHK) constant field equation (see Materials and Methods) with values of intra- and extracellular K^+ concentrations (125 mM and 8 mM, respectively) for the recording conditions. Difference (red) I-V relation in ***B*** obscures control curve (gray). Equilibrium potentials (0 current potentials, $ELeak_K$, vertical dashed lines) of currents induced by acid and halothane are identical and near E_K.

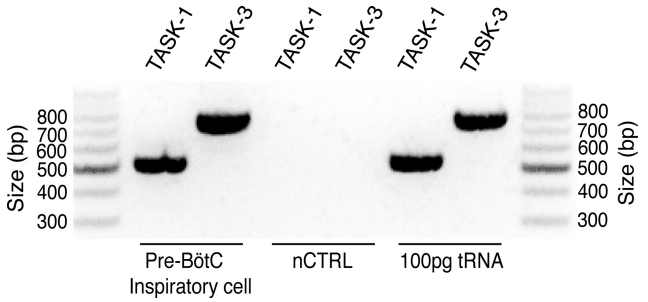

Figure 4. Pre-BötC inspiratory neurons contain TASK-1 and in some cases TASK-3 mRNA. Electrophoresis gel generated by scRT-PCR from mRNA in cytoplasm aspirated from this inspiratory neuron (intrinsic burster) shows TASK-1 (column 2) and TASK-3 (column 3) cDNA. The band for TASK-1 corresponds to the TASK-1 reference [column 6, positive control from 100 pg of total rat brain RNA (tRNA)] and to the predicted molecular weight of amplimers of TASK-1 (512 bp, column at left). The band for TASK-3 corresponds to the TASK-3 reference (column 7 positive control) and to the predicted molecular weight of amplimers of TASK-3 (763 bp). No TASK-1 or TASK-3 signals were present in negative controls (nCTR, columns 4 and 5 in this example) from 'mock harvests.'

Pre-BötC inspiratory neurons contain TASK mRNA

TASK mRNA has been shown to be present by *in situ* hybridization in adult rat pre-BötC neurons (Washburn et al., 2003) reputed to be respiratory neurons via their coexpression of neurokinin-1 receptors (Gray et al., 1999), which is not an exclusive marker for pre-BötC respiratory neurons (Gray et al., 2001; Pagliardini et al., 2005). The pre-BötC region has a heterogeneous neuronal composition with many nonrespiratory neurons, requiring electrophysiological identification of respiratory neurons. We therefore assayed for TASK channel mRNA in cytoplasm harvested during whole-cell recording from identified pre-BötC inspiratory neurons including cells with intrinsic bursting properties ($n = 14$ inspiratory neurons total, with 4 intrinsic bursters and 10 nonintrinsically bursting neurons assayed). Cytoplasm was aspirated into the pipette, and assays by scRT-PCR were performed for TASK-1 mRNA in one group of cells ($n = 9$) or for both TASK-1 and TASK-3 mRNA in another group ($n = 5$). TASK-1 mRNA was found in six of the nine pre-BötC inspiratory neurons assayed in the first group (with two of three intrinsic bursters and four of six nonintrinsic bursters tested expressing TASK-1 mRNA). TASK-1 and TASK-3 mRNA were found together in two of five cells assayed in the other group of inspiratory neurons (one of two intrinsic bursters and one of three nonintrinsic bursters tested in this group expressed both TASK-1 and TASK-3 mRNA) (Fig. 4). For any TASK-expressing inspiratory neuron assayed, no TASK-1 or TASK-3 signals were detected in negative controls from "mock harvests" in the slice (see Materials and Methods).

Intrinsic bursting of pre-BötC inspiratory neurons is modulated by acid

Does the TASK-like leak conductance regulate intrinsic rhythmic bursting behavior of pre-BötC neurons? We predict that acid, by decreasing K^+ leak conductance of pre-BötC bursters, causes depolarization, resulting in an increase in intrinsic voltage-dependent bursting frequency (Butera et al., 1999a; Del Negro et al., 2001). To test this prediction, inspiratory neurons were isolated from synaptic input by bath-applied Cd^{2+} (200 μM) to identify NaP-dependent intrinsic bursting (Koizumi and Smith, 2008), and bursting behavior of identified neurons was recorded in whole-cell current-clamp. For these experiments we used blind whole-cell patch-clamping procedures (Koizumi et al., 2008) to include in the sample neurons deeper in the slice than could be resolved by our optical imaging approaches. For voltage-clamp

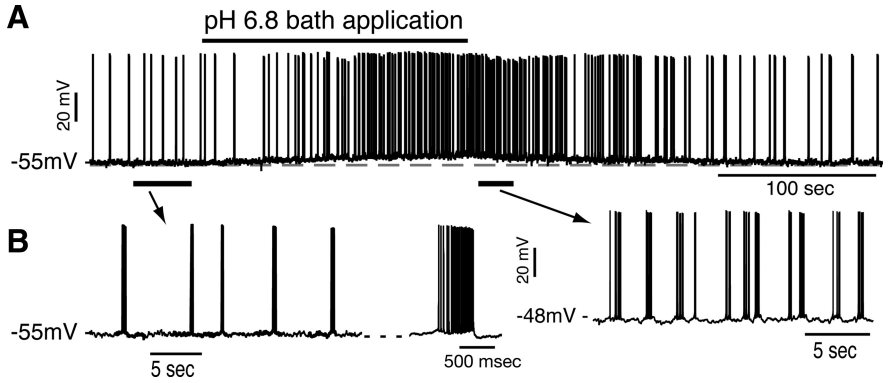

Figure 5. Modulation of intrinsic bursting frequency of pre-BötC inspiratory neurons by acid. ***A***, Current-clamp recording illustrating that transiently applied acidic aCSF (pH 6.8) reversibly depolarizes (maximally by ~7 mV in this example) and increases the baseline voltage-dependent rhythmic bursting frequency of a representative intrinsic burster synaptically isolated after blocking Ca^{2+} channels with Cd^{2+} (200 μM). ***B***, Traces with expanded time scale show bursting patterns before and during (epochs indicated by solid bars and arrows) bath application of acidic aCSF.

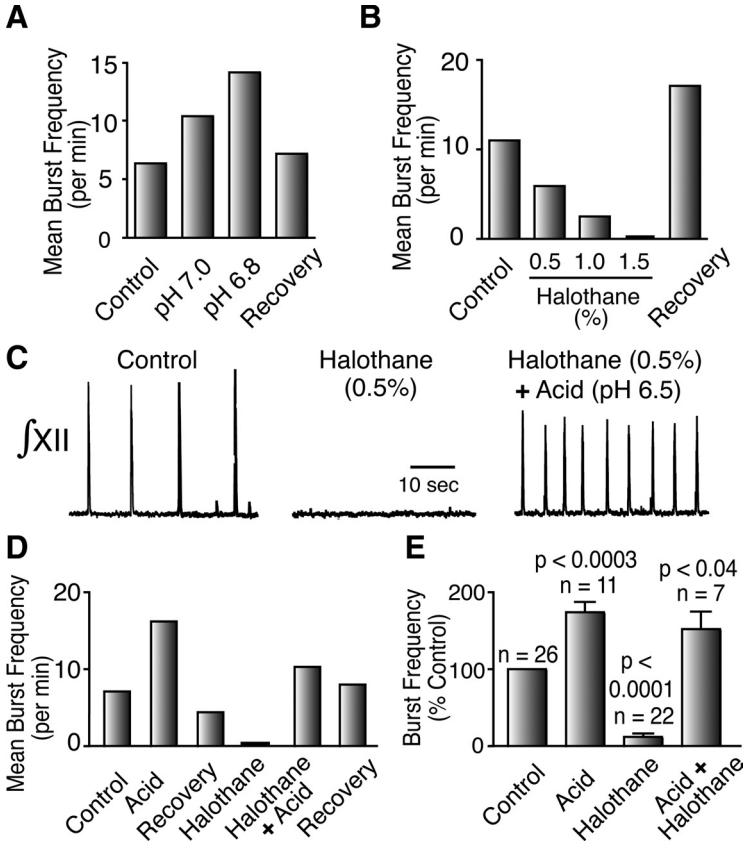

Figure 6. Modulation of respiratory network inspiratory bursting frequency in vitro by acid, halothane, and modulatory interactions of acid and halothane. ***A***, ***B***, Examples of progressive and reversible increase of inspiratory XII motoneuronal bursting frequency with acidic aCSF pH (***A***), and reversible decrease in bursting frequency with progressive increments of aCSF halothane concentrations (0.5% to 1.5%) (***B***) from two representative slices. Bars represent mean steady-state burst frequencies (bursts/min) averaged over 10 to 20 consecutive bursts at levels of aCSF pH or halothane concentration indicated. ***C***, Example of rectified, integrated hypoglossal nerve inspiratory discharge (∫XII) showing elimination of rhythmic bursting by halothane and restoration of bursting by coapplied acid (pH 6.5) in the continued presence of halothane. ***D***, Example of a full diagnostic sequence for involvement of TASK-like channels in control of network rhythm by acid and halothane. Acidic aCSF (pH 6.5) increased steady-state inspiratory burst frequency, halothane (0.5% after recovery from acid) decreased burst frequency, and acid (pH 6.5) dominated over halothane to increase burst frequency above control. ***E***, Summary data of steady-state XII burst frequency (% control) during slice exposure to acid, halothane, and acid + halothane averaged over multiple slice experiments. Acid (pH 7.0 to 6.5, $n = 11$ slices pooled) increased mean inspiratory burst frequency, halothane (0.5% to 2.0%, $n = 22$ slices pooled) decreased burst frequency, and the effect of acid dominates over that of halothane when slices were exposed to both halothane and acid ($n = 7$ slices pooled). Bars are mean values and error bars are +SE.

measurements Na^+ currents were also blocked with TTX (1 μM). In correspondence with the overall population of inspiratory neurons as described above, with exposure of the slice to acidic (pH 6.8) aCSF, gLeak of all intrinsic bursters tested ($n = 19$) decreased in this group of inspiratory cells from a mean value of 2.6 ± 0.7 nS at control pH 7.4 to 2.1 ± 0.6 nS ($p = 0.0001$) as determined from the slope of the linear fit to the ramp I-V curves at hyperpolarized voltages (<−65 mV). The average reduction in gLeak (20% from control values) with acidification in this group of intrinsic bursters was similar to that obtained for the group of intrinsic bursters and nonintrinsic bursters (24% to 26% reduction in average gLeak, pooled data) described above that were recorded at more superficial locations in the slices. Furthermore, in another group of intrinsic burster neurons tested ($n = 16$) under current clamp recording, consistent with the hypothesis that TASK-like leak conductance regulates cellular rhythmic bursting, decreasing aCSF pH from pH 7.4 to pH 6.8 depolarized the baseline membrane potential (from −49.5 ± 5.5 mV to −44.0 ± 6.0 mV, $p = 0.0001$) (Fig. 5) and increased the averaged maximum neuronal bursting frequency (from 0.1 ± 0.03 Hz to 0.2 ± 0.09 Hz, $p = 0.00039$).

Modulation of network rhythm by acid and halothane is consistent with involvement of TASK in regulation of rhythm generation

Network-wide modulation in the slice

Based on our results that TASK-like leak regulates rhythmogenesis at the cellular level, we analyzed modulation of inspiratory rhythm by acid and halothane at the network level, monitored by XII motor population discharge. Halothane-containing aCSF applied to the slice monotonically decreased steady-state inspiratory discharge frequency and terminated rhythmic network activity, in a concentration-dependent manner, and terminated rhythmic network activity ($n = 22$ slices) (Fig. 6*B*,*C*,*E*). Acidic aCSF applied to the slice increased XII discharge frequency ($n = 11$, 178 ± 44% of control, $p < 0.0003$ at pH 6.8) (Fig. 6*A*,*E*), and diagnostic of involvement of TASK channels in modulation of the rhythm reactivated rhythmic network activity in the presence of halothane ($n = 7$) (Fig. 6*C–E*). The effect of acid (pH 6.8) dominated over the effect of halothane when halothane and acid were applied together: the acid-induced increase of XII discharge frequency (174 ±

74% of control, $p < 0.04$, $n = 7$) in the presence of halothane was nearly as large as the frequency increase by acid alone (Fig. 6*E*).

Modulation at the level of the pre-BötC network

To establish whether modulation of network rhythm by acid and halothane involved perturbations of neuronal excitability at the level of the pre-BötC network, acidic or halothane-containing aCSF was bilaterally microinfused directly into the core of the imaged pre-BötC (Fig. 1, $n = 5$ slices). This circumvented the possibility of network-wide modulation of rhythm by neurons outside of the pre-BötC in the slice that may be acid/halothane sensitive and can modulate pre-BötC neuron excitability. There is TASK in hypoglossal motoneurons (Talley et al., 2000), and also in raphé nuclei (Washburn et al., 2002), which have chemosensory properties (Richerson, 2004; Mulkey et al., 2007) and excitatory serotonergic neuronal projections to pre-BötC and hypoglossal respiratory neurons (Ptak et al., 2009). Microinfusion of acidic aCSF (pH 7.2, 7.0, 6.8, 6.0) bilaterally into the core of the pre-BötC increased the frequency of XII inspiratory discharge (Fig. 7*A–C*). The onset of elevation of burst discharge frequency was faster than when the slice was superfused with acidic solution. Quantitatively, the acid-induced increase in discharge frequency was dose-dependent (Fig. 7*C*) with a maximal mean increase of 225% above control at pH 6.0. The calculated Hill slope of the pH versus frequency relation was 0.84. Bilateral microinfusion of halothane-containing aCSF (2% in pipette solution, $n = 4$) progressively decreased XII burst frequency and terminated rhythm generation, whereas bath-applied acidic aCSF (pH 6.8, $n = 5$) reversed the halothane induced slowing of network rhythm (Fig. 7*D*,*E*).

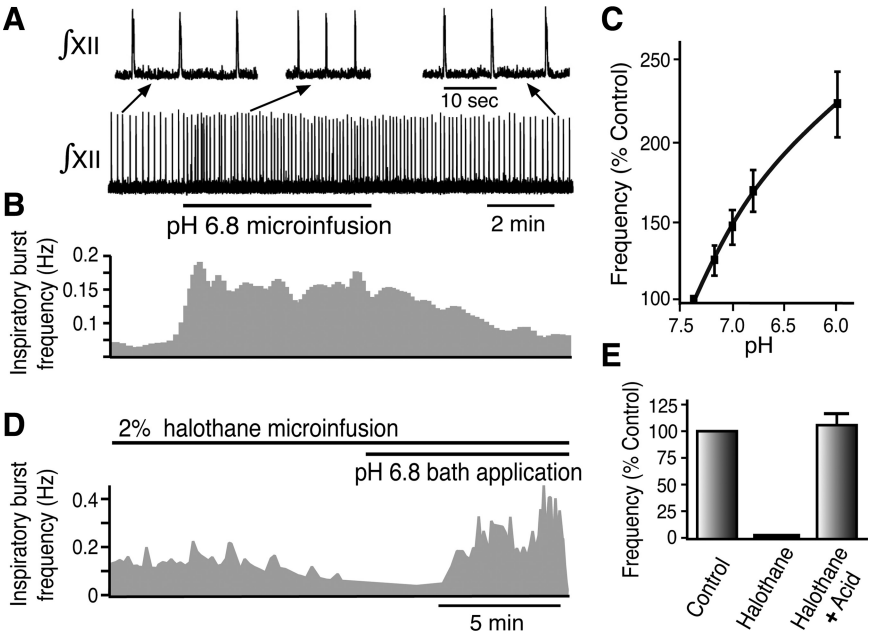

Figure 7. Modulation of inspiratory rhythm by acid and halothane at the level of the pre-BötC network. ***A***, Continuous microinfusion of acidic aCSF (pH 6.8, bar) bilaterally into the pre-BötC directly increased inspiratory burst frequency recorded from hypoglossal nerves (∫XII shown). Expansion of selected sections of ***A*** showing acid-induced increase of burst frequency, followed by return to control frequency, are shown at top. ***B***, Inspiratory burst frequency versus time plot for ***A***, continuously computed by taking the inverse of each interburst interval and smoothing with a three-point binomial filter. ***C***, Data as in ***A*** pooled from five slices and four values of pH of aCSF separately microinfused into the pre-BötC in each slice. Network bursting frequency increased monotonically with progressive local acidification. Solid line is a Hill equation fit to the data points with a Hill slope of 0.84. Error bars represent ±SD. ***D***, Example of burst frequency versus time plot as in ***B*** computed for this slice by averaging the inverse of every two interburst intervals. Halothane (2% in aCSF solution) microinfused into the pre-BötC nearly stopped network rhythmic activity, whereas acidic aCSF (pH 6.8) applied in the bath during halothane microinfusion reversed the depressant effect of halothane and elevated network-bursting frequency above control values. ***E***, Sequence of halothane and acid application as in ***D*** summarizing pooled results from multiple slice experiments ($n = 4$). In all slices halothane (2%) microinfused into the pre-BötC progressively reduced, and in 3 slices stopped, network rhythmic activity, whereas acidic aCSF (pH 6.8) subsequently bath-applied during halothane microinfusion reversed the effect of halothane and elevated bursting frequency above control levels. Bars are mean values and error bars are +SE.

TASK-like component of neuronal leak regulates rhythm generation in pre-BötC neuron and network model simulations

To further investigate the link between modulation of TASK-like leak conductance at the cellular level and modulation of rhythmic bursting activity at cellular and network levels, we analyzed control of rhythm by a K^+ leak conductance in single neuron models of intrinsically bursting pre-BötC cells (Butera et al., 1999a; Purvis et al., 2007) and a rhythmic excitatory network model of the pre-BötC (Butera et al., 1999b; Purvis et al., 2007), consisting of a heterogeneous mixture of 50 intrinsically bursting and non-intrinsically bursting model neurons (Butera et al., 1999b; Purvis et al., 2007; Koizumi and Smith, 2008). Neurons in these models had voltage-clamp ramp I-V relations and leak conductances similar to those measured experimentally here and elsewhere (Purvis et al., 2007; Koizumi and Smith, 2008). The total neuronal leak conductance, gLeak, was partitioned into a K^+ conductance component ($gLeak_K$) and a smaller non-K^+ mixed cationic conductance component (see Modeling methods), which we estimated is ~10% of gLeak under basal condition. We analyzed modulation of rhythmic cellular/network activity as the neuronal K^+ component was varied over a range of values predicted from the measured gLeak in whole-cell voltage-clamp recording and changes in $gLeak_K$ with acidic and halothane conditions. Because the voltage-activated persistent Na^+ current (NaP) dynamically interacts in the neuronal model with the leak current (Koizumi and Smith, 2008), simulations of the models were run over the normal range of single neuron NaP conductance (gNaP) measured in pre-BötC inspiratory neurons in neonatal rat slices *in vitro* (Purvis et al., 2007; Koizumi and Smith, 2008) to examine the modulatory role of $gLeak_K$ for a range of possible cellular/network initial conditions.

Single model neurons

We first analyzed the behavior of a model intrinsically bursting pre-BötC neuron as the single-cell $gLeak_K$ was varied (Fig. 8). In the parameter space covering the experimentally measured values of gNaP, values of gLeak (here and Purvis et al., 2007), and estimated values of $gLeak_K$, the single-neuron model (Butera et al., 1999a) was well behaved in that for a given gNaP, neuronal bursting frequency decreased monotonically to 0 Hz with increasing $gLeak_K$ (Fig. 8*A*,*B*), and the range of burst frequencies (0 to 0.35 Hz) covered the experimentally observed range. The single neuron model was bounded by $gLeak_K = 2.0$ nS, below which

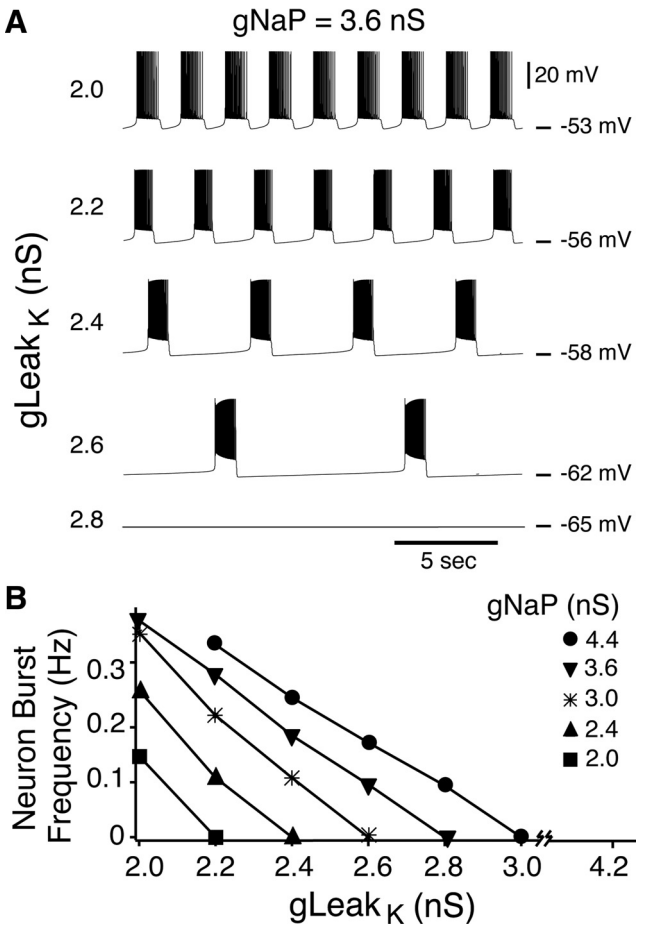

Figure 8. Bursting behavior of a model pre-BötC intrinsically bursting neuron modulated by changes in the K^+ component ($gLeak_K$) of the total leak conductance. ***A***, Example simulation of rhythmic bursts of single neuron model when gNaP was set to 3.6 nS, near the upper end of the range of gNaP for pre-BötC intrinsic bursters (***B***). Traces are membrane potential versus time for simulated current-clamp recording conditions. Progressively increasing TASK-like $gLeak_K$ (from top to bottom simulation traces), corresponding to an increase in halothane concentration, progressively reduces neuronal burst frequency and ultimately stops rhythmic bursting (bottom). ***B***, Summary plots of simulated relations between $gLeak_K$ and model neuron bursting frequency for different gNaP isopleth values covering the range of gNaP values (2.0 to 4.4 nS) found experimentally in pre-BötC intrinsically bursting inspiratory neurons (Purvis et al., 2007; Koizumi and Smith, 2008). The range of estimated $gLeak_K$ (2.0 to 7.0 nS) covers the measured experimental range of TASK-like K^+ leak conductance with modulation by acid (lower end of range) and halothane (upper end). Model neuron burst frequency versus $gLeak_K$ over experimental range of gNaP shows that burst frequency is inversely proportional to $gLeak_K$ for all values of gNaP. The model neuron bursts rhythmically in the parameter range $gLeak_K = 2.0$ to 3.0 nS and gNaP = 2.0 to 4.4 nS. At $gLeak_K$ below 2.0 nS, outside of the range of $gLeak_K$ estimated for acidic conditions in the present experiments, the neuron spikes tonically, whereas above $gLeak_K = 4.0$ nS (halothane conditions) the neuron is silent over the range of gNaP values.

the model neuron spikes tonically at a given gNaP, and by gNaP = 2.0 nS, below which the model neuron is silent at a given $gLeak_K$. The estimated mean value of $gLeak_K$ for pre-BötC intrinsic bursters for acidic conditions (~2.0 nS at pH 6.8), when plotted on the gNaP isopleths of 2.4 nS or 3.6 nS, which bound most of the measured range for gNaP in pre-BötC intrinsic bursters (Purvis et al., 2007), yielded a range of burst frequencies similar to that recorded here from intrinsic bursters under acidic conditions (0.2 to 0.3 Hz). For simulated halothane conditions (estimated $gLeak_K$ = ~6.0 to 7.0 nS), the model is silent (not intrinsically bursting) for any value of gNaP. Thus modulation of a TASK-like $gLeak_K$, mimicking experimentally observed average ranges of $gLeak_K$ obtained with acid and halothane, yielded in the model a dynamic range of burst frequencies typical of that recorded from single intrinsically bursting pre-BötC neurons.

Model networks

For network simulations, we distributed estimated values of neuronal $gLeak_K$ to yield a mean population value ($GLeak_K$) with SD ± 30% for a 50-neuron population to model the heterogeneous population of pre-BötC neurons consisting of a mixture of intrinsic and nonintrinsically bursting inspiratory neurons. The statistical distribution of gLeak values conformed with that found experimentally here and previously (Purvis et al., 2007) for a mixed population of pre-BötC inspiratory cells. Network simulations (Koizumi and Smith, 2008), in which $GLeak_K$ was varied over the range corresponding to mean values of $gLeak_K$ obtained for acidic and halothane conditions, exhibited a range of burst frequencies similar to that observed experimentally (from data summarized in Fig. 6, and network frequencies shown in Fig. 7), 0 to ~0.5 Hz (Fig. 9*A*,*B*). For a given value of population mean NaP conductance (GNaP, also distributed over the population with ±30% SD, see Materials and Methods), the network burst frequency decreased monotonically to zero with increasing $GLeak_K$. The estimated value of $GLeak_K$ of 3.5 nS for the general population of inspiratory neurons (intrinsic bursters and nonintrinsic bursters) under control conditions, coupled with the GNaP value of 2.4 nS measured previously (Purvis et al., 2007), yielded in the model network simulations burst frequencies of ~0.15 Hz, similar to bursting frequencies recorded from the slice network under control conditions. For the range of $GLeak_K$ values (2.5 to 3.0 nS) estimated for acidic conditions for the general population, with a GNaP of 2.4 nS, a network bursting frequency range of ~0.3 to 0.5 Hz obtained in the model simulations, covering the frequency range observed experimentally during slice perfusion or pre-BötC microinfusion of acidic aCSF. Over the estimated range of $GLeak_K$ with network exposure to halothane (6.0 to 7.0 nS), network burst frequency is zero, consistent with our observations for the rhythmic slice during halothane superfusion or pre-BötC microinfusion. Thus our network simulation results suggest that modulation of a cellular TASK-like K^+ leak conductance can be directly expressed as modulatory effects on rhythm at the network level.

Discussion

We obtained evidence for TASK channels within inspiratory neurons of the pre-BötC by scRT-PCR and established electrophysiologically that TASK-like channels are functional in pre-BötC cells. Our cellular-level voltage-clamp measurements for both intrinsic and nonintrinsically bursting pre-BötC inspiratory neurons satisfied the four diagnostic properties of TASK channels differentiating these channels from all other known channels: selectivity for K^+, I-V relations described by constant field theory, channel closure to extracellular acid, and channel opening to halothane. Our single-cell recordings furthermore showed that pre-BötC inspiratory neurons are depolarized and intrinsically bursting neurons accordingly exhibited increased bursting frequencies with exposure to acid as predicted for contributions of TASK to gLeak. Finally, the inspiratory bursting frequency of the pre-BötC network is modulated by acid and halothane, consistent with the cellular-level changes in gLeak measured and also predicted by our computational models with modulation by the K^+ component of leak conductance.

TASK-like channels contribute to leak conductance of neurons of the pre-BötC inspiratory rhythm generator

Pre-BötC neurons exhibit a classic leak conductance at membrane voltages below those at which nonlinear voltage-dependent conductances activate (here and Koizumi and Smith, 2008). Ramp I-V relations were essentially linear over this subthreshold voltage range, and after blocking voltage-activated conductances the I-V relations over a wider voltage range exhibited weak outward rectification. We tested for the signature dual responses of TASK to acid and halothane (Lesage and Lazdunski, 2000; Talley and Bayliss, 2002) and demonstrated reduced gLeak with exposure to acid and an augmented conductance by halothane that could be completely reversed by acid. Furthermore, I-V relations for the acid- and halothane-associated conductances had reversal potentials near E_k and conformed to predictions from the GHK constant field equation for K^+ channels. All of these characteristics are consistent with properties of TASK channels. We note however that although these biophysical and pharmacological criteria to identify TASK channels are standard with proven reliability, many of these same criteria have been used to implicate functional involvement of TASK channels in some neurons, particularly for glucose sensing in orexin neurons (Burdakov et al., 2006), but this conclusion was subsequently proven incorrect (Guyon et al., 2009; Gonzalez et al., 2009). Thus definitive molecular identification of TASK channels in pre-BötC neurons based on the above criteria remains tentative.

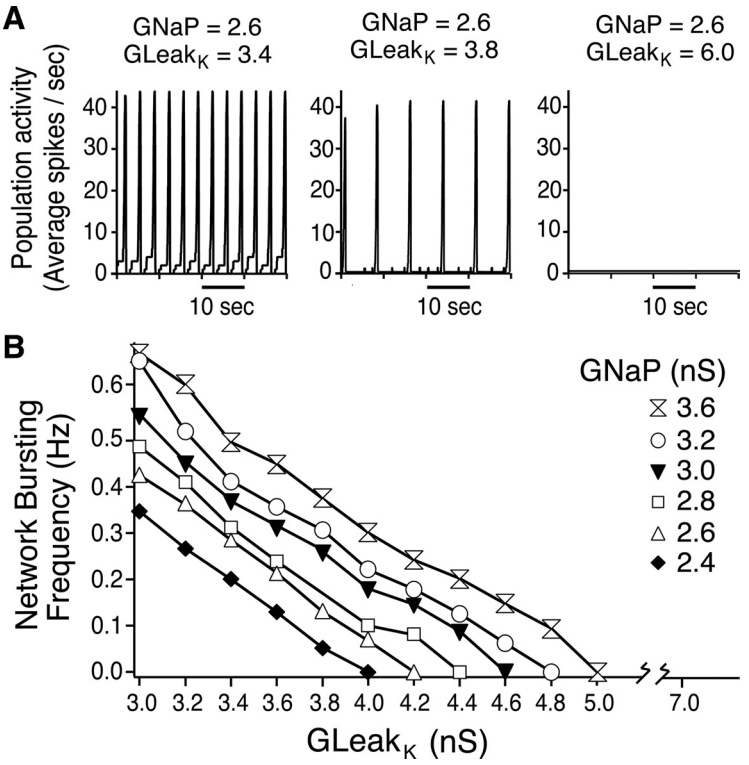

Figure 9. Modulation of rhythmic bursting behavior by population TASK-like K^+ leak conductance in a model heterogeneous neuronal excitatory network of the pre-BötC. Simulation results shown are for a 50 excitatory neuron network model with a range of mean population K^+ leak values ($GLeak_K$ = 2.0 to 7.0 nS) covering the average range estimated from single neurons with acid and halothane modulation of $GLeak_K$. The simulated population had a range of GNaP (2.0 to 4.4 nS population mean values) as measured previously for a population of pre-BötC inspiratory neurons (Purvis et al., 2007; Koizumi et al., 2008) (for simplicity only simulation results for GNaP = 2.4 to 3.6 nS are shown). ***A***, Example of model network simulation output when population GNaP was set for illustration to 2.6 nS (± 30%SD) and $GLeak_K$ was varied from 3.4 to 6.0 nS (± 30% SD). Shown are population-spiking activity histograms (50 ms bins) averaged over the 50 individual network neurons. Population burst frequency decreases as $GLeak_K$ increases, ultimately stopping network rhythmic activity, mimicking effects at the network level of halothane on TASK-like leak conductance. ***B***, Summary plots of model relations between $GLeak_K$ and population bursting frequency for a range of fixed values of GNaP. For any value of GNaP, population-bursting frequency was inversely proportional to $GLeak_K$, and network activity could be stopped at higher values of $GLeak_K$. Below GNaP = 2.2 nS, the model network was silent. For GNaP = 2.4 to 3.6 nS, the network model exhibited rhythmic population bursting when $GLeak_K$ was between 2.4 to 4.8 nS (for simplicity only simulation results with $GLeak_K$ values above 3.0 nS are shown). For estimated $GLeak_K$ during exposure of the slice or pre-BötC to halothane (6.0 to 7.0 nS), the model network was silent, reproducing experimental results. See text for further explanation.

Do K^+ channels other than TASK-1 and TASK-3 contribute to the modulation of leak conductance by acid? G-protein-coupled inwardly rectifying K^+ channels (Kir) can modulate inspiratory rhythm generation *in vitro* (Johnson et al., 1996), and at least three types of Kir channels, Kir 2.3 (Zhu et al., 1999), Kir 4.1, and Kir 4.1–5.1 (Xu et al., 2000), are acid sensitive. Kir 4.1 conductance decreases in response to acid with a pK of 6.2 matching that of TASK-3, and Kir 4.1–5.1 conductance decreases in response to acid with a pK of 7.4 matching TASK-1, whereas the pK for Kir 2.3 is intermediate at 6.8. However, the sensitivity of these Kirs is to intracellular, not extracellular, acid. The pH of our whole-cell recording pipette solution was strongly buffered at 7.3 to 7.4 with HEPES. Furthermore, because the acid-modulated leak I-V relations in our measurements were outwardly and not inwardly rectifying and conductance changes obtained were unaffected by Kir blockers, Kir likely did not mediate acid-induced changes in $gLeak_K$. Channels linked to putative chemosensory purinergic (P2) receptors are also unlikely to be involved because these receptors do not mediate chemosensory responses of pre-BötC cells (Lorier et al., 2007; Funk et al., 2008).

In our whole-cell recordings a nonrectifying leak conductance persisted even at an acidification of pH 6.5 (data not shown). Because TASK-1 channels are almost entirely closed at pH 6.5 (Berg et al., 2004), this residual conductance is not from TASK-1. The pK for TASK-3 is ~6.5 (Berg et al., 2004), so the residual conductance could be attributable to TASK-3. This inference is supported by our preliminary results from a small number of slices (n = 3) showing that isoflurane (0.5%), which specifically blocks TASK-3 (Berg et al., 2004), reduces network bursting frequency to nearly zero. Furthermore, we found that the pH range over which microinfusion of acid into the pre-BötC monotonically increased inspiratory bursting frequency extended to pH 6.0.

Network-level modulation of rhythm generation by TASK-like channels

Our experimental analyses show that halothane down-regulated, and extracellular acid augmented, network-level inspiratory bursting frequency when these TASK modulators were either bath applied or directly microinfused bilaterally into the pre-BötC. Furthermore, our computational results suggest how modulation of a TASK-like K^+ component of leak conductance, distributed over a model heterogenous excitatory network of neurons with subthreshold I-V relations dominated by Leak and

NaP (here and Koizumi and Smith, 2008), can account for our experimental observations. Reducing or augmenting $GLeak_K$, respectively, causes neuronal depolarization or hyperpolarization within the network with concomitant increases or decreases in population-wide bursting frequency over a dynamic range similar to that observed experimentally. Taken together with our cellular-level analysis, the experimental and computational results suggest that modulation of a TASK-like K^+ leak conductance can be directly expressed as modulatory effects on inspiratory rhythmic activity at the network level. Although our results with local microinfusion of halothane and acid into the pre-BötC are consistent with predictions based on our cellular measurements and model simulations, we note that we cannot exclude the possibility that in some experiments the suppression of network activity by local halothane and its subsequent reversal by reduced pH (Fig. 7*D*,*E*) could involve different channels in different neurons, especially because the reversal of local halothane effects were obtained with bath acidification. At present, however, we favor the most parsimonious explanation that the perturbations of network inspiratory activity observed are due to TASK channel modulation in pre-BötC neurons.

TASK and other leak channels as targets for modulation of pre-BötC rhythm generation

Because TASK channels are instantly activating, noninactivating, outwardly rectifying, and are selective for K^+, most investigators in the K_{2P} channel field immediately inferred that TASK provides a K^+ component of neuronal leak conductance. Butera et al. (1999a,b) originally proposed that the ohmic-like leak current of neurons constituting the pre-BötC inspiratory rhythm generator is K^+-dominated and provides a basic mechanism for modulation of rhythm generation at cellular and network levels. Meuth et al. (2003) provided the first experimental evidence that TASK channels are a component of leak currents controlling activity of a neural rhythm generator. Here we present evidence that TASK channels provide a K^+ leak conductance-based mechanism for chemosensory-related modulatory control of pre-BötC rhythm generation.

A number of neurotransmitters with G-protein-coupled receptors close TASK channels (Bayliss et al., 2003; Mathie, 2007). In recombinant systems, TASK closes in response to TRH (Talley and Bayliss, 2002), angiotensin II (Czirjak et al., 2000), and muscarinic M1 receptor agonists (Czirjak et al., 2001). Other neurotransmitters, including substance P (SP), serotonin (5-HT), norepinephrine, and glutamate (acting via metabotropic glutamate receptors) also close a leak conductance that has TASK-like acid and halothane sensitivity (Talley et al., 2000). Thus as proposed for other neurons (Bayliss et al., 2003; Mathie, 2007), TASK channels may constitute a convergent target for neuromodulatory control of pre-BötC rhythm generation. SP and 5-HT have been shown to augment pre-BötC cellular and network bursting by reducing a TASK-like K^+ component of leak conductance in pre-BötC inspiratory neurons (Koizumi and Smith, 2008; Ptak et al., 2009), although these neuromodulators act simultaneously via other cationic components of leak, such as a NALCN-like component (Ptak et al., 2009), that also cause neuronal excitation. Thus there appears to be duality in modulatory control involving several channel entities comprising discrete leak conductance components of which TASK represents one important set of K^+ background channels.

Recent studies with TASK-1 and TASK-3 knockout mice (Mulkey et al., 2007; Trapp et al., 2008) have not demonstrated abnormal baseline breathing *in vivo*, although TASK-1 knockouts show abnormal ventilatory responses to hypoxia and moderate hypercapnia, attributed to peripheral (Trapp et al., 2008) but not some critical central brainstem chemoreceptive cells (Mulkey et al., 2007). TASK-1 should normally be open at physiological pH, but the observations of normal baseline breathing in the knockout mice may imply that: (1) other K^+ background channels are also major components of the K^+-dominated leak of pre-BötC neurons; (2) other K^+ channel components are upregulated in these knockouts, including in cells involved in chemoreception that may exhibit compensatory changes is spontaneous firing behavior (Trapp et al., 2008) to regulate activity of the respiratory network by afferent input to the pre-BötC and other network components; and (3) other leak channels such as NALCN that normally comediate modulatory actions of neuromodulators such as SP and 5-HT, which critically control pre-BötC network excitability (Ptak et al., 2009), are sufficient for neuromodulatory control. K^+ channel candidates that may be other normal components of leak or are upregulated include other K_{2P} channels such as TWIK (Lesage et al., 1996), TREK (Fink et al., 1996), and TRAAK (Fink et al., 1998), or a yet unknown background K^+ channel(s).

In summary, we have presented evidence that a component of the K^+-dominated leak conductance of pre-BötC neurons is mediated by TASK-like channels. Accordingly, TASK may constitute a convergent target for modulatory control of pre-BötC rhythm generation, including by regulatory signals associated with CO_2/H^+ as well as neuromodulators that critically control pre-BötC rhythmic activity.

References

Bayliss DA, Siros JE, Talley EM (2003) The TASK family: two-pore-domain background K^+ channels. Mol Interven 3:205–219.

Berg AP, Talley EM, Manger JP, Bayliss DA (2004) Motoneurons express heteromeric TWIK-related acid-sensitive K+ (TASK) channels containing TASK-1 (KCNK3) and TASK-3 (KCNK9) subunits. J Neurosci 24:6693–6702.

Burdakov D, Jensen LT, Alexopoulos H, Williams RH. Fearon IM, O'Kelly I, Gerasimenko O, Fugger L, Verkhratsky A (2006) Tandem-pore K^+ channels mediate inhibition of orexin neurons by glucose. Neuron 50:711–722.

Butera RJ Jr, Rinzel J, Smith JC (1999a) Models of respiratory rhythm generation in the pre-Botzinger complex. I. Bursting pacemaker neurons. J Neurophysiol 82:382–397.

Butera RJ Jr, Rinzel J, Smith JC (1999b) Models of respiratory rhythm generation in the pre-Botzinger complex. II. Populations of coupled pacemaker neurons. J Neurophysiol 82:398–415.

Chen KC, Nicholson C (2000) Spatial buffering of potassium ions in brain extracellular space. Biophys J 78:2776–2797.

Czirjak G, Fischer T, Spat A, Lesage F, Enyedi P (2000) TASK (TWIK-related acid-sensitive potassium channel) is expressed in glomerulosa cells of rat adrenal cortex and inhibited by angiotensin II. Mol Endocrin 14:863–874.

Czirjak G, Petheo GL, Spat A, Enyedi P (2001) Inhibition of TASK-1 potassium channel by phospholipase C. Am J Physiol Cell Physiol 281:C700–C708.

Del Negro CA, Johnson SM, Butera RJ, Smith JC (2001) Models of respiratory rhythm generation in the pre-Botzinger complex. III. Experimental tests of model predictions. J Neurophysiol 86:59–74.

Del Negro CA, Koshiya N, Butera RJ Jr, Smith JC (2002) Persistent sodium current, membrane properties and bursting behavior of pre-botzinger complex inspiratory neurons in vitro. J Neurophysiol 88:2242–2250.

Duprat F, Lesage F, Fink M, Reyes R, Heurteaux C, M. L (1997) TASK, a human background K^+ channel to sense external pH variations near physiological pH. EMBO J 16:5464–5471.

Feldman JL, Del Negro CA (2006) Looking for inspiration: new perspectives on respiratory rhythm. Nat Rev Neurosci 7:232–242.

Filosa JA, Dean JB, Putnam RW (2002) Role of intracellular and extracellu-

lar pH in the chemosensitive response of rat locus coeruleus neurones. J Physiol 541:493–509.
Fink M, Duprat F, Lesage F, Reyes R, Romey G, Heurteaux C, Lazdunski M (1996) Cloning, functional expression and brain localization of a novel unconventional outward rectifier K^+ channel. EMBO J 15:6854–6862.
Fink M, Lesage F, Duprat F, Heurteaux C, Reyes R, Fosset M, M L (1998) A neuronal two P domain K^+ channel stimulated by arachidonic acid and polyunsaturated fatty acids. EMBO J 17:3297–3308.
Funk GD, Huxtable AG, Lorier AR (2008) ATP in central respiratory control: a three-part signaling system. Respir Physol Neurobiol 164:131–142.
Gonzalez JA, Jensen LT, Doyle SE, Miranda-Anaya M, Menaker M, Fugger L, Bayliss DA, Burdakov D (2009) Deletion of TASK1 and TASK3 channels disrupts intrinsic excitability but does not abolish glucose or pH responses of orexin/hypocretin neurons. Eur J Neurosci 30:57–64.
Gray PA, Rekling JC, Bocchiaro CM, Feldman JL (1999) Modulation of respiratory frequency by peptidergic input to rhythmogenic neurons in the preBotzinger complex. Science 286:1566–1568.
Gray PA, Janczewski WA, Mellen N, McCrimmon DR, Feldman JL (2001) Normal breathing requires preBotzinger complex neurokinin-1 receptor-expressing neurons. Nat Neurosci 4:927–930.
Guyon A, Tardy MP, Rovere C, Nahon J-L, Barhanin J, Lesage F (2009) Glucose inhibition persists in hypothalamic neurons lacking tandem-pore K^+ channels. J Neurosci 29:2528–2533.
Hayes JA, Del Negro CA (2007) Neurokinin receptor-expressing pre-Bötzinger complex neurons in neonatal mice studied *in vitro*. J Neurophysiol 97:4215–4224.
Hille B (2001) Ionic channels of excitable membranes, Third Edition. Sunderland, MA: Sinauer Associates.
Johnson SM, Smith JC, Feldman JL (1996) Modulation of respiratory rhythm in vitro: Role of Gi/o-protein regulated mechanisms. J Appl Physiol 80:2120–2133.
Johnson SM, Koshiya N, Smith JC (2001) Isolation of the kernel for respiratory rhythm generation in a novel in vitro preparation: the pre-Bötzinger complex "island". J Neurophysiol 85:1772–1776.
Koizumi H, Smith JC (2008) Persistent Na^+ and K^+-dominated leak currents contribute to respiratory rhythm generation in the Pre-Botzinger complex in vitro. J Neurosci 28:1773–1785.
Koshiya N, Smith JC (1999) Neuronal pacemaker for breathing visualized in vitro. Nature 400:360–363.
Leonoudakis D, Gray A, Winegar B, Kindler C, Harada M, Taylor D, Chavez R, Forsayeth J, Yost C (1998) An open rectifier potassium channel with two pore domains in tandem cloned from rat cerebellum. Neuroscience 18:868–877.
Lesage F, Guillemare E, Fink M, Duprat F, Lasdunski M, Romey G, Barhanin J (1996) TWIK-1, a ubiquitous human weakly inward rectifying K^+ channel with a novel structure. EMBO J 15:1004–1011.
Lesage F, Lazdunski M (2000) Molecular and functional properties of two-pore-domain potassium channels. Am J Physiol Renal Physiol 279:F793–F801.
Lorier AR, Huxtable AG, Robinson DM, Lipski J, Housley DM, Funk GD (2007) P2Y1 receptor modulation of the pre-Bötzinger complex inspiratory hrythm generating network in vitro. J Neurosci 27:993–1005.
Lu B, Su Y, Das S, Liu J, Xia J, Ren D (2007) The neuronal channel NALCN contributes resting sodium permeability and is required for normal respiratory rhythm. Cell 129:371–383.
Lu B, Su Y, Das S, Wang H, Wang Y, Liu J, Ren D (2009) Peptide neurotransmitters activate a cation channel complex of NALCN and UNC-80. Nature 457:741–744.
Mathie A (2007) Neuronal two-pore-domain potassium channels and their regulation by G protein-coupled receptors. J Physiol 578:377–385.
Medhurst AD, Rennie G, Chapman CG, Meadows H, Duckworth MD, Kelsell RE, Gloger II, Pangalos MN (2001) Distribution analysis of human two pore domain potassium channels in tissues of the central nervous system and periphery. Brain Res Mol Brain Res 86:101–114.
Meuth S, Budde T, Kanyshkova T, Broicher T, Munsch T, Pape H (2003) Contribution of TWIK-Related Acid-Sensitive K^+ Channel 1 (TASK1) and TASK3 channels to the control of activity modes in thalamocortical neurons. J Neurosci 23:6460–6469.
Mulkey DK, Talley EM, Stornetta RL, Siegel AR, West G, Cheng X, Sen N, Mistry AM, Guyenet PM, Bayliss DA (2007) TASK channels determine pH sensitivity in select respiratory neurons but do not contribute to central respiratory chemosensitivity. J Neurosci 27:14049–14058.
Nattie EE (2001) Central chemosensitivity, sleep, and wakefulness. Respir Physiol 129:257–268.
Pagliardini S, Adachi T, Ren J, Funk GD, Greer JJ (2005) Fluorescent tagging of rhythmically active neurons within the pre-Bötzinger complex of rat medullary slice preparations. J Neurosci 25:2591–2596.
Ptak K, Yamanishi T, Aungst J, Milescu L, Zhang R, Richerson GB, Smith JC (2009) Raphé neurons stimulate respiratory circuit activity by multiple mechanisms via endogenously released serotonin and substance P. J Neurosci 29:370–3737.
Purvis LK, Smith JC, Koizumi H, Butera RJ (2007) Intrinsic bursters increase the robustness of rhythm generation in an excitatory network. J Neurophysiol 97:1515–1526.
Putnam RW, Filosa JA, Ritucci NA (2004) Cellular mechanisms involved in CO(2) and acid signaling in chemosensitive neurons. Am J Physiol Cell Physiol 287:C1493–C1526.
Rajan S, Wischmeyer E, Liu G, Preisig-Muller R, Daut J, Karschin A, Derst C (2000) TASK-3, a novel tandem pore domain acid-sensitive K+ channel: an extracellular histidine as pH sensor. J Bio Chem 275:16650–16657.
Richerson GB (2004) Serotonergic neurons as carbon dioxide sensors that maintain pH homeostasis. Nat Rev Neurosci 5:449–461.
Shin KS, Rothberg BS, Yellen G (2001) Blocker state dependence and trapping in hyperpolarization-activated cation channels: evidence for an intracellular activation gate. J Gen Physiol 117:91–101.
Sirois JE, Lei Q, Talley E, Lynch C, Bayliss D (2000) The TASK-1 two-pore domain K^+ channel is a molecular substrate for neuronal effects of inhalation anesthetics. J Neurosci 20:6347–6354.
Sirois JE, Lynch C, Bayliss DA (2002) Convergent and reciprocal modulation of a leak K+ current and I(h) by an inhalational anaesthetic and neurotransmitters in rat brainstem motoneurones. J Physiol 541:717–729.
Smith JC, Ellenberger HH, Ballanyi K, Richter DW, Feldman JL (1991) Pre-Botzinger complex: a brainstem region that may generate respiratory rhythm in mammals. Science 254:726–729.
Smith JC, Butera RJ, Koshiya N, Del Negro C, Wilson CG, Johnson SM (2000) Respiratory rhythm generation in neonatal and adult mammals: the hybrid pacemaker-network model. Respir Physiol 122:131–147.
Solomon IC, Edelman NH, O'Neal MH, 3rd (2000) CO_2/H^+ chemoreception in the cat pre-Botzinger complex in vivo. J Appl Physiol 88:1996–2007.
Talley EM, Bayliss DA (2002) Modulation of TASK-1 (Kcnk3) and TASK-3 (Kcnk9) potassium channels: volatile anesthetics and neurotransmitters share a molecular site of action. J Biol Chem 277:17733–17742.
Talley EM, Lei Q, Sirois JE, Bayliss DA (2000) TASK-1, a two-pore domain K^+ channel is modulated by multiple neurotransmitters in motoneurons. Neuron 25:399–410.
Trapp S, Aller MI, Wisden W, Gourine AV (2008) A role for TASK-1 (KCNK3) channels in chemosensory control of breathing. J Neurosci 28:8844–8850.
Washburn CP, Sirois JE, Talley EM, Guyenet PG, Bayliss DA (2002) Serotonergic raphe neurons express TASK channel transcripts and a TASK-like pH- and halothane-sensitive K^+ conductance. J Neurosci 22:1256–1265.
Washburn CP, Bayliss DA, Guyenet PG (2003) Cardiorespiratory neurons of the rat ventrolateral medulla contain TASK-1 and TASK-3 channel mRNA. Respir Physiol Neurobiol 138:19–35.
Xu H, Cui N, Yang Z, Qu Z, Jiang C (2000) Modulation of Kir4.1 and Kir5.1 by hypercapnia and intracellular acidosis. J Physiol 524:725–735.
Zhu G, Chanchevalap S, Cui N, Jiang C (1999) Effects of intra- and extracellular acidifications on single channel Kir2.3 currents. J Physiol 516:699–710.